Journal of Mass Spectrometry

WILEY

Journal of MASS SPECTROMETRY

RESEARCH ARTICLE OPEN ACCESS

Surface and Subsurface Mass Spectrometric Analysis of Dexamethasone in Solid Pharmaceutical Dosage Forms

Matjaž Finšgar

Faculty of Chemistry and Chemical Engineering, University of Maribor, Maribor, Slovenia

Correspondence: Matjaž Finšgar (matjaz.finsgar@um.si)

Received: 27 March 2025 | **Revised:** 8 May 2025 | **Accepted:** 13 May 2025

Funding: This work was supported by the Slovenian Research Agency (P2-0118, J1-4416). The project is co-financed by the Republic of Slovenia, the Ministry of Higher Education, Science and Innovation, and the European Union under the European Regional Development Fund.

Keywords: active ingredient | AFM | dexamethasone | tablet analysis | ToF-SIMS | XPS

ABSTRACT

This study presents an in-depth mass spectrometric investigation of dexamethasone (DEX) distribution within pharmaceutical tablets using time-of-flight secondary ion mass spectrometry (ToF-SIMS) combined with gas cluster ion beam (GCIB) sputtering. Fragmentation mechanism of DEX was identified, which enabled the determination of three-dimensional chemical imaging of the active ingredient in both surface and subsurface regions. The data reveal that a 4-mg DEX formulation exhibits a continuous and extended distribution of the drug into the tablet matrix, while a 0.5-mg formulation shows DEX localized in distinct, isolated domains. Topographical features and the overall composition of the surface were confirmed by complementary analyses employing atomic force microscopy (AFM) and x-ray photoelectron spectroscopy (XPS). These results demonstrate how molecule distribution patterns can be linked to formulation heterogeneity using advanced mass spectrometric techniques, opening new possibilities for pharmaceutical manufacturing quality control and optimization.

1 | Introduction

Dexamethasone (DEX) is a synthetic glucocorticoid with potent anti-inflammatory and immunosuppressive properties and is, therefore, important for modern clinical practice. For example, it is used in critically ill COVID-19 patients and has significantly reduced mortality by dampening excessive inflammatory responses, even though the exact molecular mechanisms remain under investigation. Beyond its role in respiratory distress situations, DEX is a key component of therapeutic regimens in various oncological settings. In hematologic malignancies such as B cell acute lymphoblastic leukemia and multiple myeloma, it induces apoptosis and enhances the efficacy of combination therapies. However, recent studies have highlighted complexities, such as the paradoxical activation of survival pathways that may contribute to drug resistance. Its application in managing brain metastases further highlights its utility. Perioperative administration alongside stereotactic radiosurgery has been shown to modulate local immune responses and improve patient outcomes. The versatility of DEX extends to innovative drug delivery approaches. Advances in implant technology now allow for controlled, sustained release of corticosteroids, potentially enhancing therapeutic efficacy while minimizing systemic side effects. Its applications from acute infectious and inflammatory conditions to chronic and neoplastic diseases demonstrate the critical need for further research. A deeper understanding of its diverse cellular effects will enable the refinement of dosing strategies and the development of novel delivery systems, ultimately optimizing its therapeutic potential. In general, the central role of DEX lies in reducing mortality in severe inflammatory conditions and complex action in oncological therapies [1–7].

Determining the exact spatial distribution of DEX within solid pharmaceutical forms (e.g., tablets) is essential for understanding

its clinical performance. Even minor variations in the localization of the active ingredient can significantly affect drug release kinetics and stability, ultimately influencing therapeutic outcomes. By employing appropriate methods, researchers can correlate the tablet's surface features with its clinical efficacy, paving the way for more effective formulation strategies and improved patient care.

Conventional analytical techniques, such as dissolution tests, which only provide bulk concentrations, are unable to provide the degree of detail that surface analytical techniques do when it comes to the heterogeneous distribution of active components and excipients in solid dosage forms. Due to the fact that differences in component distribution might affect medication release patterns, stability, and overall therapeutic performance, this spatial information is essential. High-resolution chemical imaging of tablet surfaces is made possible by methods such as time-of-flight secondary ion mass spectrometry (ToF-SIMS), as opposed to wet analytics, which dissolve the entire sample and so lose any locational context. The very few reports in the literature indicate that ToF-SIMS is rarely used to investigate solid pharmaceutical forms, despite its potential to the show molecular-level distribution patterns essential for formulation optimization and quality control [8–16]. Only a few studies were reported that used ToF-SIMS for DEX investigation. ToF-SIMS was used to perform depth profiling to track the distribution of characteristic DEX ion signals within the scaffolds. In the scaffolds without sucrose acetate isobutyrate, the DEX signal was located at the surface but dropped significantly with depth, indicating that the drug was mainly localized at the surface. In contrast, the ToF-SIMS analysis for scaffolds containing sucrose acetate isobutyrate showed a more homogeneous DEX distribution [17]. ToF-SIMS was also used to map the spatial distribution of DEX sodium phosphate within ocular tissues following intravitreal injection. This analysis enabled the visualization of the drug located in the lens, vitreous humor, and retina [18].

X-ray photoelectron spectroscopy (XPS) can provide quantitative elemental and chemical state information from the sample's topmost position a few nanometers in depth, thus offering high surface sensitivity. Because changes in oxidation states, bonding conditions, or chemical interactions at the tablet surface might affect drug release patterns, stability, and overall therapeutic performance, this level of control is crucial [19].

Moreover, nanoscale resolution of the surface topography is not possible with conventional analytical methods but can be studied by atomic force microscopy (AFM). The latter is particularly important for tablet analysis. Surface heterogeneities that can have a substantial impact on a tablet's stability and performance, such as microstructural flaws, recrystallization events, and phase transitions, can be directly visualized by AFM. It can offer data that is essential for manufacturing and formulation process optimization. Recent research has shown that AFM is useful in ensuring consistent product quality and improved therapeutic efficacy by monitoring surface crystallization in cocrystal compacts and evaluating the impact of processing-induced disorder on tablet surfaces [20–23].

This study shows the surface characteristics of DEX tablets by comparing formulations with differing drug concentrations from different manufacturers by employing 3D profilometry, AFM, XPS, and ToF-SIMS. Additionally, gas cluster ion beam (GCIB) sputtering was used for nondestructive depth profiling, enabling the investigation of the active ingredient and the excipients throughout the tablet matrix.

2 | Experimental

2.1 | The Samples and Standard for Surface Analysis

The DEX tablets contained 4 mg of DEX (hereinafter referred to as 4-mg DEX tablets) and were obtained from a pharmacy in Maribor, Slovenia. According to the manufacturer, the DEX tablet's excipients included lactose, corn starch, SiO_2, and Mg stearate, although their exact concentrations were not specified.

Lactose serves as a filler to add bulk, corn starch functions as a binder and a disintegrant, SiO_2 acts as a glidant and anticaking agent, while magnesium stearate is used as a lubricant to facilitate tablet manufacturing.

For comparison, tablets containing 0.5-mg DEX were also analyzed (hereinafter referred to as 0.5-mg DEX tablets). They were obtained from a pharmacy in Berlin, Germany. The reported excipients (by the manufacturer) were lactose monohydrate, carboxymethyl starch sodium (disintegrant), hydroxypropyl cellulose (binder), Mg stearate, and SiO_2. The content of these excipients was also not reported.

For all analyses, both the 4-mg DEX tablet and the 0.5-mg DEX tablet, the entire tablets were used without any pretreatment, such as cutting. The tablets were removed from the aluminum blisters by cutting the foil along the edge, ensuring no direct contact with the tablet surface. Each tablet was then positioned on the holder for analysis without touching the surface.

DEX reference standard (white powder, US Pharmacopeia reference standard, pharmaceutical primary standard) was purchased from Sigma-Aldrich. This DEX reference standard was pressed to obtain a DEX tablet of the standard (hereinafter referred to as DEX standard) 5 mm in diameter and approximately 2 mm thick using an Atlas 25 T hydraulic press (Specac, Orpington, United Kingdom).

2.2 | 3D Profilometry and AFM Measurements

Large area surface topography analysis and the determination of the depth of the craters formed after GCIB sputtering using XPS and ToF-SIMS were performed using a DektakXT stylus profilometer (Bruker, Karlsruhe, Germany). After the 3D profile acquisition, a software operation termed form removal was performed using Mountains Map Imaging Topography (Digital Surf, Besançon, France). This was done to flatten the concave or convex shapes of the tablet surfaces.

An MFP 3D Origin Plus (Asylum/Oxford Instruments, Santa Barbara, California, United States) was used for the AFM

analyses. The measurements were conducted in tapping mode utilizing OMCL-AC240TS-C3 cantilevers coated with reflective aluminum (Olympus), with a resonant frequency of 70 kHz, a spring constant of 1.7 N/m, and a scan rate of 0.65–0.75 Hz. The images were measured with a resolution of 256 by 256 pixels. Igor Pro software was employed to generate AFM images.

2.3 | XPS Measurements

XPS measurements were performed by means of a Supra+ device (Kratos, Manchester, United Kingdom) using an Al K_α excitation source. The spectra were corrected using the C-C/C-H peak located at 284.8 eV in the C 1s spectra. Charge compensation was performed using a neutralizer. XPS acquisition and data processing were performed using ESCApe 1.5 software (Kratos). The 4-mg DEX tablet, 0.5-mg DEX tablet, and the DEX standard were attached to the sample holder using double-sided Si-free tape. The spectra were measured at a 90° take-off angle at a spot size of 110 μm in diameter. High-resolution and survey spectra were measured at 40 and 160-eV pass energy, respectively. Depth profiling was performed with 10-keV Ar_{1000}^+ GCIB sputtering targeting a 2 by 2 mm spot size. Shirley background correction was performed for quantification.

GCIB sputtering was employed to remove surface layers of organic materials chemically nondestructively. GCIB sputtering minimizes damage to the organic compounds, preserving their molecular integrity during depth profiling. Such sputtering is essential for analyzing both the active ingredients and excipients in pharmaceutical tablets using XPS and ToF-SIMS techniques.

2.4 | ToF-SIMS Measurements

ToF-SIMS measurements were conducted using an IONTOF M6 instrument (IONTOF, Münster, Germany). The 4-mg DEX tablet, 0.5-mg DEX tablet, and DEX sample were mounted in a top-mount sample holder. To counteract charging effects during measurements, a flood gun was employed. A 30-keV Bi_3^+ primary ion beam with a 0.6-pA target current, generated by a Nanoprobe 50 liquid metal ion gun (LMIG), was used for analysis. The surface potential was adjusted as required depending on the analyzed spots. Mass spectra were calibrated using known secondary ion peaks at defined mass-to-charge (m/z) ratios: $C_3H_7^+$ (m/z 43.05), $C_4H_7^+$ (m/z 55.05), $C_5H_9^+$ (m/z 69.07), and $C_8H_9^+$ (m/z 105.07).

Depth profiling was performed using 10-keV Ar_{2000}^+ GCIB sputtering with a target current of 10 nA. GCIB sputtering was executed over a 500 by 500 μm area, with simultaneous analysis focused on a 200 by 200 μm region at the center of the sputtered area. Data acquisition and processing, including multivariate curve resolution (MCR) analysis, were conducted using SurfaceLab 7.3. MCR calculations employing a random initialization approach and an arbitrarily small epsilon value as a convergence criterion.

3 | Results and Discussion

Surface characterization is essential for elucidating pharmaceutical formulations' microstructure and chemical heterogeneity. In this study, a combination of 3D profilometry, AFM, XPS, and ToF-SIMS was employed because each technique contributes distinctively to understanding the tablets' physical and chemical properties. 3D profilometry and AFM provide detailed information on surface topography (also morphological information) and roughness, while XPS and ToF-SIMS reveal elemental and molecular compositions. Incorporating GCIB sputtering further allows for the chemically nondestructive removal of surface layers, which is critical for preserving the integrity of organic compounds during depth profiling.

A comparative analysis of a 4-mg DEX tablet and a 0.5-mg DEX tablet was performed for two primary reasons. First, it is aimed at evaluating the impact of varying drug concentrations on tablet composition and surface characteristics, which can influence drug release and stability. Second, as these tablets originate from different manufacturers, the study also examines how distinct formulation practices affect the distribution of the active ingredient and excipients. For the scientific community, such analyses can provide valuable insights into formulation optimization, quality control, and the relationship between tablet microstructure and therapeutic performance, ultimately supporting the development of more consistent and effective pharmaceutical products.

Figure 1 presents 3D surface topography profiles (Figure 1a,b) and AFM images (Figure 1c,d) for the 4-mg DEX tablet (Figure 1a,c) and for the 0.5-mg DEX tablet (Figure 1b,d). Based on the 3D profiles in Figure 1a,b (measurement on three different tablets), the average mean surface roughness (S_a) ± standard deviation values were calculated to be 1.844 ± 0.264 μm for the 4-mg DEX tablet and 2.211 ± 0.061 μm for the 0.5-mg DEX tablet, suggesting minor differences in surface roughness.

The height (topography) and amplitude images from the AFM analysis offer a comprehensive view of the surface morphology. Darker regions in these images signify lower regions (valleys), whereas brighter areas indicate elevated features. A rougher surface, with distinct peaks and valleys, suggests irregular material deposition or phase separation, potentially affecting tablet uniformity. On the other hand, a smoother surface indicates a more homogeneous excipient distribution, which may enhance drug stability and dissolution characteristics.

Both the 4-mg DEX tablet and the 0.5-mg DEX tablet exhibit relatively rough surfaces, highlighting differences in excipient distribution. The presence of heterogeneous regions suggests phase separation or uneven material dispersion. Figure 1c,d and Figures S1–S4 (Supporting Information) show that the structural components at different places of the tablets vary significantly, ranging from a few nanometers to several hundred nanometers, contributing to the surface morphology differences.

Below, the XPS and ToF-SIMS analyses provide insights into the chemical composition of the tablets. The XPS measurements

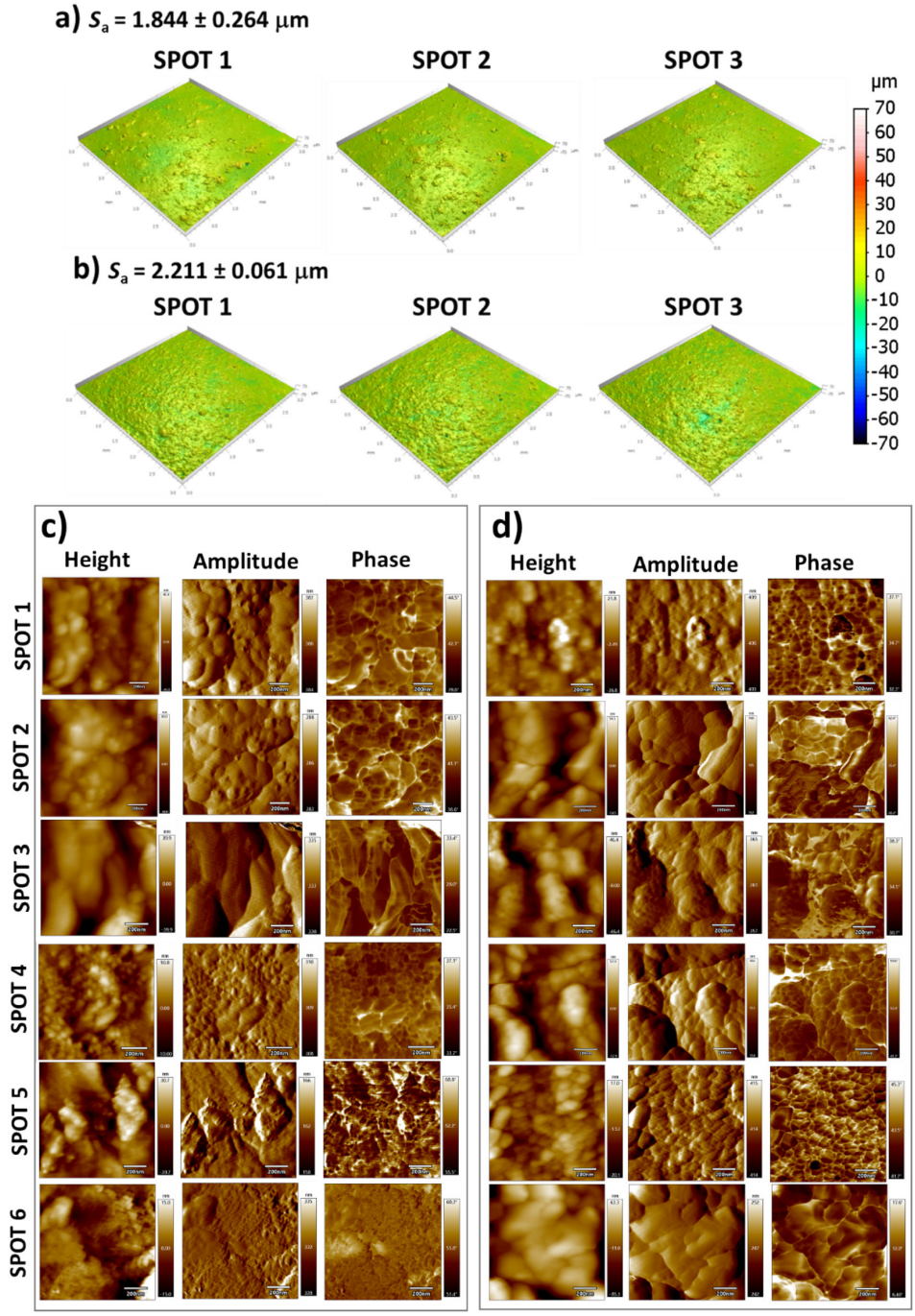

FIGURE 1 | (a, b) 3D surface topography profiles measured over a 3 by 3 mm area and (c, d) AFM images acquired from six different spots over a 1 by 1 µm area. The images in (a, c) correspond to the 4-mg DEX tablet, and the images in (b, d) correspond to 0.5-mg DEX tablet, highlighting differences in surface topography, morphology, and roughness. The scale bar represents 200 nm.

detail the elemental composition and chemical states present on the surface, highlighting variations in C, O, Si, and F signals, among others. Simultaneously, ToF-SIMS provides complementary molecular-specific information by identifying characteristic ion fragments associated with DEX and the excipients.

Figure 2 presents the XPS results. The dashed-line spectra in Figure 2a–c,g represent the survey and high-resolution spectra measured on the DEX standard after 10 min of 10-keV Ar_{1000}^+ GCIB sputtering, which was employed to eliminate potential surface contaminants before XPS analysis (to remove adventitious carbonaceous species). For the 4-mg DEX tablet, the solid-line spectra were collected before and after sputtering over specified time intervals (with each sputtering duration indicated in Figure 2h) in order to generate a depth profile. The highest spectra in Figure 2 correspond to a location 15 µm beneath the surface of the 4-mg DEX tablet, as determined by 3D profilometry by measuring the depth of the sputter crater.

The survey spectra in Figure 2a show signals for C 1s, O 1s, F 1s, Si 2s, Si 2p, and Mg 2p, along with XPS-excited Auger signals (O KLL and F KLL).

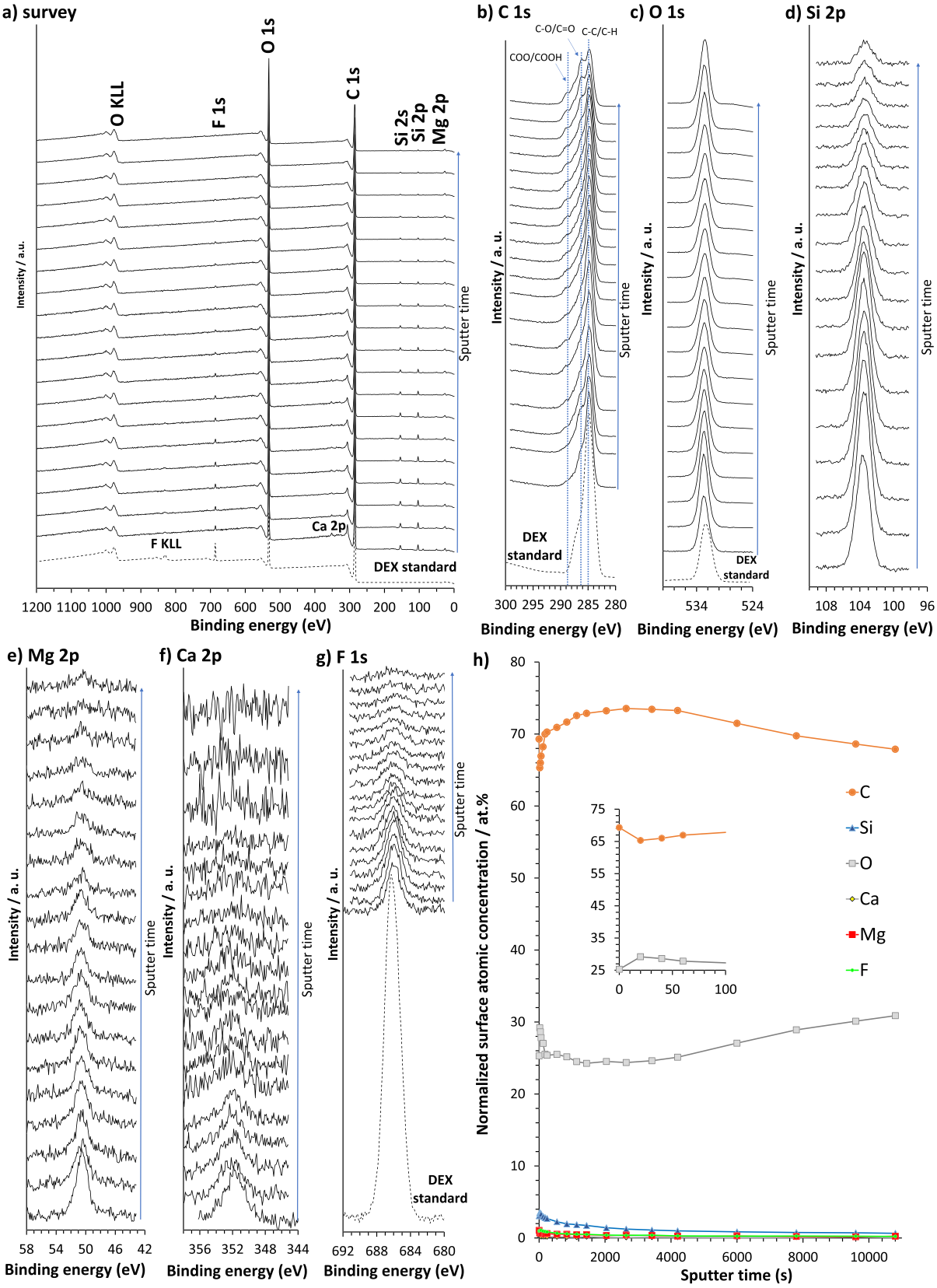

FIGURE 2 | XPS (a) survey and high-resolution (b) C 1s, (c) O 1s, (d) Si 2p, (e) Mg 2p, (f) Ca 2p, and (g) F 1s spectra. The lowest spectra (solid lines) represent the surface before sputtering; sputtering is represented by the spectra from the bottom up. (h) The surface atomic concentration determined during depth profiling using 10-keV Ar_{1000}^{+}. The depth after 10 800 s of GCIB sputtering was determined using 3D profilometry to be 15 μm. The lowest spectra represented by the dashed lines in (a–c, g) describe the measurement of the DEX standard.

The C 1s signal originates from DEX and organic excipients in the 4-mg DEX tablet. For the topmost position—the lowest spectra (solid lines) in Figure 2a,b—the C 1s signal can also originate from adventitious carbonaceous species adsorbed on the tablet's surface. The removal of adventitious carbonaceous species by GCIB sputtering is also indicated in the insert of Figure 2h, where the surface atomic concentration of C decreases by about 4 at.% after the first sputtering cycle for 20 s (simultaneously, the surface atomic concentration of O increases by about 4 at.%). No such sudden significant change was present when the surface was sputtered further (Figure 2h). On the other hand, Figure 2b shows three different C environments, that is, C-C/C-H at 284.8 eV, C-O/C=O at approximately 286.5 eV, and COO/COOH at approximately 289.0 eV. The C-C/C-H can originate from Mg stearate, C-O/C=O can originate from lactose and corn starch, and COO comes from Mg stearate. Figure 2b shows that the spectral feature corresponding to C-O/C=O becomes more intense with an increase in sputter time, most likely as more lactose and corn starch were reached when the topmost layers were gradually removed.

The O 1s signal can originate from DEX, lactose, corn starch, Mg stearate, or SiO_2, while for the topmost position—the lowest spectra for the 4-mg DEX tablet—the O 1s signal can also originate from adventitious oxidized carbonaceous species adsorbed on the tablet's surface. The position of the O 1s signal for SiO_2 is at approximately 533 eV [24], which also corresponds to the position of the O 1s signal for oxygen from organic compounds. This makes the differentiation of these species difficult using XPS. No significant change in the intensity and peak position of the O 1s spectra is present in Figure 2c by comparing the spectra for the DEX standard and O 1s spectra for the 4-mg DEX tablet measured before and after sputtering. However, the surface atomic concentration of O changes with sputter time (Figure 2h), which is a consequence of the change in the surface atomic concentration of other elements, as these concentrations are determined by normalization to 100.0 at.%.

Si 2s and Si 2p originate from SiO_2 (Figure 2a,d). The position of the Si 2p peak corresponds to SiO_2 at a binding energy of 103.3 eV [24, 25]. The shape of the Si 2p spectra is similar by going deeper into the subsurface region (Figure 2d); however, the intensity of this peak drops significantly, indicating that SiO_2 is mainly present at the topmost position of the sample.

For the XPS measurements of the topmost positions, Mg 2p and Ca 2p signals were also developed (the lowest spectra in Figure 2e,f). The Mg 2p signal gradually decreases with sputter time, while the signal for Ca 2p disappears after the fifth sputtering cycle (after 120 s). The latter suggests that Mg stearate and Ca-containing species are more abundant in the topmost positions.

F 1s and XPS-excited Auger F KLL originate from DEX molecules as they contain F (as shown in Figure 3). The intensity of the F 1s signal is high for the DEX standard as it contains only DEX. Compared to the DEX standard, the intensity of the F 1s signal for the 4-mg DEX tablet is lower as it also contains other excipients on the surface; thereby, the surface concentration of DEX is lower, producing a less intense signal for F 1s (Figure 2g). By means of GCIB sputtering of the 4-mg DEX tablet, the signal for F 1s decreases (Figure 2a,g), indicating that most of the DEX is located on the topmost position of the 4-mg DEX tablet. However, as represented below in the 3D ToF-SIMS images, the agglomeration density of DEX depends on the location on the 4-mg DEX tablets.

In addition to the detailed XPS analysis of the 4-mg DEX tablet (Figure 2), a similar investigation was carried out on the 0.5-mg DEX tablet. The survey and high-resolution spectra for the 0.5-mg tablet (shown in Figure S5) reveal notable differences in the elemental composition compared to the 4 mg tablet.

Compared to the 4-mg DEX tablet, the 0.5-mg DEX tablet exhibits additional Na- and Cl-containing species. For the 0.5-mg DEX tablet, Cl 2p and Cl 2s peaks appear in the survey spectra of deeper subsurface regions (the upper spectra in Figure S5a), indicating that chlorine content increases with sputtering time.

Furthermore, the surface of the 0.5-mg DEX tablet shows a higher proportion of oxidized carbonaceous species (as seen in the lowest spectra in Figure S5b) relative to its deeper subsurface regions (the upper spectra in Figure S5b). This behavior is in contrast with that of the 4-mg DEX tablet (Figure 2b), which highlights a compositional difference between the two formulations.

In the 0.5-mg DEX tablet, the O, Si, and Mg concentrations decrease with sputtering (Figure S5c–e,i), while the shape and position of the O 1s, Si 2p, and Mg 2p spectra remain unchanged. This consistency suggests that the chemical environments of these elements are preserved throughout the sputtering process.

Additionally, the topmost surface of the 0.5-mg DEX tablet exhibits a Ca 2p peak (the lowest spectra in Figure S5f), confirming the presence of Ca. Due to the lower DEX content in the 0.5-mg DEX tablet, the surface atomic concentration of fluorine is lower. For such a low F content, the F 1s peak was not detected during the entire sputtering procedure (Figure S5g). However, ToF-SIMS later confirms the presence of DEX in the 0.5-mg DEX tablet as this technique has lower detection limits compared to XPS. Moreover, as the 0.5-mg DEX tablet contains carboxymethyl starch sodium, Na 1s and XPS-excited Na KLL peaks were detected (Figure S5a,h), with Na content increasing with sputtering time (Figure S5h). Furthermore, similarly as found for the 4-mg DEX tablet, a decrease in C content and a corresponding increase in O content after the first sputtering cycle are evident for the 0.5-mg DEX tablet, likely due to the removal of adventitious carbonaceous species from the surface (see the insert in Figure S5i).

Next, ToF-SIMS was utilized to provide molecular-specific information that supplements the elemental and topographical/morphological insights gathered by XPS, 3D profilometry, and AFM. First, characteristic ion fragments that act as molecular fingerprints for DEX and the excipients were determined. The assignment of signals for analytes is made possible due to molecular specificity, which enables tablets to be imaged in three dimensions and the mapping of the spatial distribution of DEX and excipients throughout the tablet matrix. Since it is difficult to accomplish such 3D molecular imaging using other analytical techniques, ToF-SIMS is an essential tool for establishing a

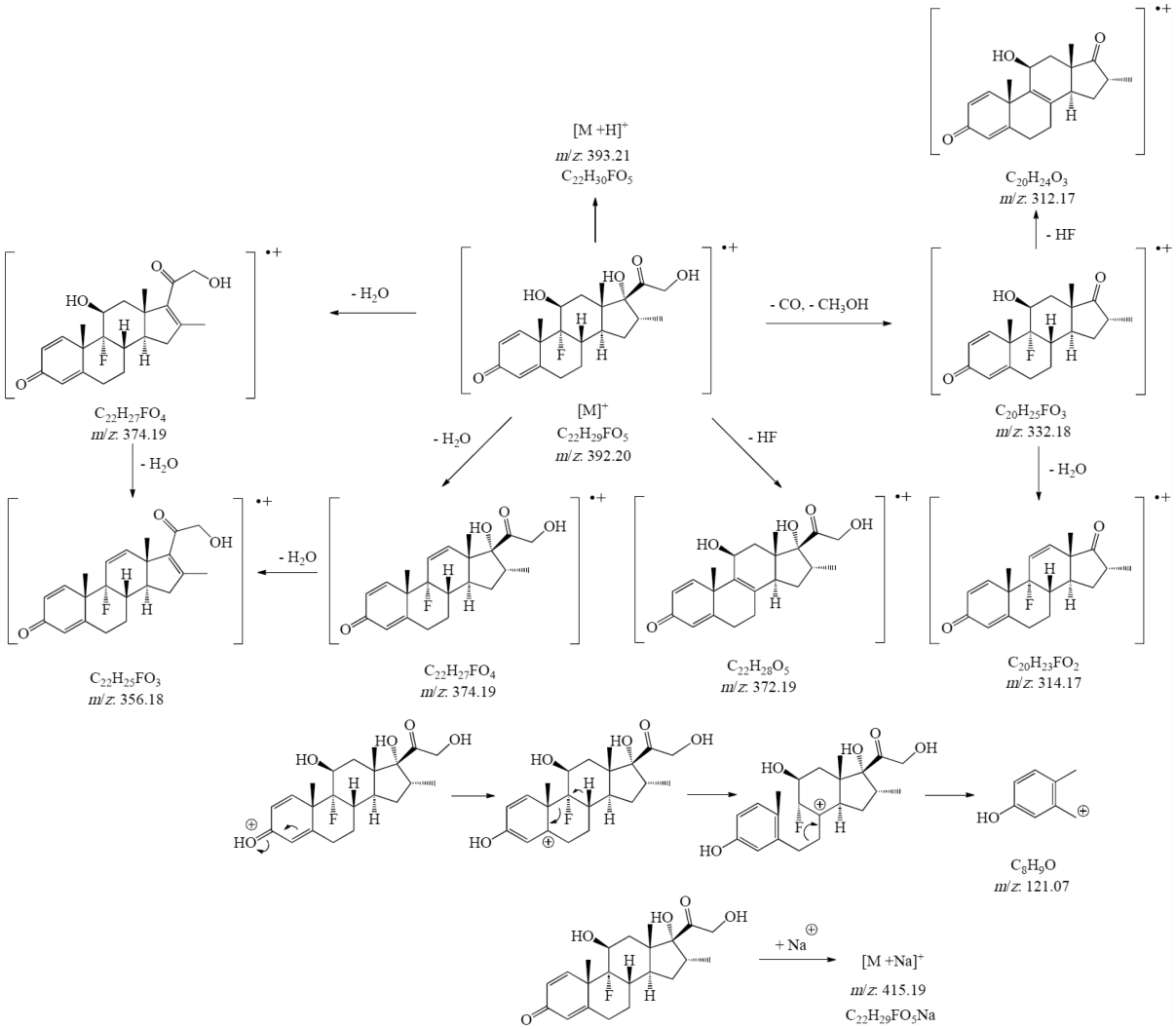

FIGURE 3 | Suggested fragmentation pattern for DEX with fragments whose signals were confirmed in the ToF-SIMS spectra (Figure 4).

correlation between the chemical composition and the spatial arrangement of tablet components.

Figure 3 shows the proposed fragmentation pathway of DEX using ToF-SIMS. The assigned ion fragments were confirmed by comparing theoretical fragmentation patterns with the ToF-SIMS spectra presented in Figure 4.

The parent ion ($[M]^+$, i.e., $C_{22}H_{29}FO_5^+$) has an m/z of 392.20 (Figure 4j), which upon protonation forms $[M+H]^+$, that is, $C_{22}H_{30}FO_5^+$ at m/z 393.21 (Figure 4k). The fragmentation of $[M]^+$ involves the loss of H_2O, resulting in $C_{22}H_{27}FO_4^+$ at m/z 374.19 (Figure 4i). Subsequently, H_2O is eliminated, producing a $C_{22}H_{25}FO_3^+$ at m/z 356.18 (Figure 4g). However, $[M]^+$ can fragment also by the loss of HF, resulting in $C_{22}H_{28}O_5^+$ at m/z 372.19 (Figure 4h). Additional fragmentation of M^+ involves the loss of CO and CH_3OH forming $C_{20}H_{25}FO_3^+$ at m/z 332.18 (Figure 4f). The fragmentation continues in two manners, with the loss of H_2O forming $C_{20}H_{23}FO_2^+$ at m/z 314.17 (Figure 4e) or with the loss of HF forming $C_{20}H_{24}O_3^+$ at m/z 312.17 (Figure 4d). The fragmentation of steroid DEX results also in a well-known fragmentation with ring cleavage producing $C_8H_9O^+$ at m/z 121.07 (Figure 4c) [26–31]. In addition, signals that confirm the dimer of DEX and protonated DEX dimer were detected at m/z 784.41 and 785.42 (Figure 4l,m), respectively. Moreover, the signal for the adduct of $[M]^+$ with Na was detected, that is, $C_{22}H_{29}FO_5Na^+$ at m/z 415.19 (Figure 4n) [32–36].

Moreover, the analysis of 3D ToF-SIMS images using the above-mentioned signals for DEX consistently showed that all signals colocalize at the same positions across six distinct spots—three tablets with two analyzed spots each. This consistent spatial correlation strongly suggests that these fragments originate from DEX, thereby reinforcing the specificity of the molecular signals for DEX.

Next, MCR processing was performed to determine the MCR factor corresponding to DEX. MCR factors represent distinctive patterns from complex datasets that correspond to the individual components present in a sample. These MCR factors enable differentiation between the various ingredients within the tablet. By isolating these MCR factors, we can identify molecular-specific signals characteristic of analytes. Furthermore, as spectral interferences can occur, uniqueness analysis was performed. This means that the characteristic signals previously

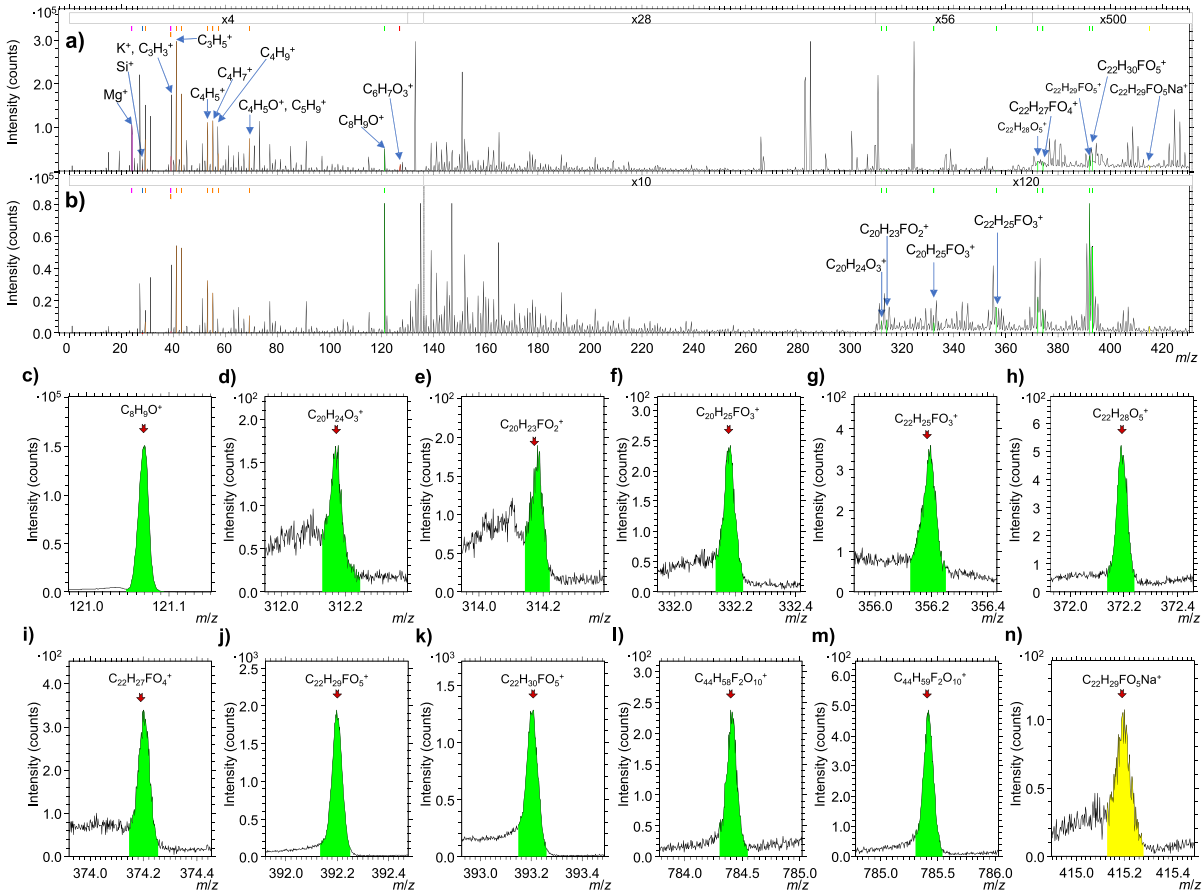

FIGURE 4 | Wide-range ToF-SIMS spectra for (a) the 4-mg DEX tablet and (b) the DEX standard; a detailed view of the ToF-SIMS spectra measured for (c–m) the DEX standard and for (n) the 4-mg DEX tablet showing the signals as predicted in Figure 3. The red arrows in (c–n) show the theoretical m/z position of the corresponding signals. Spectra were acquired after 600 s of sputtering on an area of 500 by 500 μm using a 10-keV Ar_{2000}^{+} to remove adventitious carbonaceous species.

associated with the MCR factor corresponding to DEX were checked to determine if they contribute solely to this MCR factor, and if they do, they are considered unique [11, 37]. This differentiation confirms that the detected peaks are inherent to DEX, allowing for the exact mapping of its distribution within the tablet.

An analysis to determine the uniqueness of signals was performed, and signals corresponding to m/z 121.07, 354.18, 372.19, 374.19, 392.20, and 393.21 were determined to be unique. The signal at m/z 121.07, corresponding to $C_8H_9O^+$, was the most intense among all characteristic signals for DEX (unique and nonunique signals). Based on that, $C_8H_9O^+$ was selected to perform 3D imaging to show the spatial distribution of DEX in the DEX tablets.

Figure 5 shows the distribution of 4-mg DEX tablet ingredients, that is, DEX, saccharides (lactose and starch), SiO_2, and Mg stearate. DEX, saccharides, SiO_2, and Mg stearate are represented by the signals for $C_8H_9O^+$, $C_6H_7O_3^+$, Si^+, and Mg^+, respectively. A signal for $C_6H_7O_3^+$ at m/z 127.05 is a characteristic of saccharides such as allose, glucose, fructose, mannose, and galactose [38]. As lactose is a disaccharide made of glucose and galactose and starch is a polysaccharide made of glucose, $C_6H_7O_3^+$ was used as a marker to map the distribution of these two excipients (it is also for cellulose, made from glucose, as given in Figure S6).

The DEX-specific signal, represented by the signal for $C_8H_9O^+$, is predominantly located in the upper layers but extends into subsurface regions up to 40-μm deep. In contrast, a saccharide-related signal—attributed to lactose and starch—is more evenly distributed below the surface rich components. The signals for SiO_2 and Mg stearate, identified through Si^+ and Mg^+, are mainly concentrated at the surface but are also visible at deeper subsurface regions. This spatial variation indicates that the manufacturing process may lead to nonuniform mixing or compression, which can affect the tablet's dissolution and drug release properties. Overall, the 3D imaging confirms that the active ingredient and excipients are not uniformly distributed throughout the tablet, offering critical insights into formulation quality and performance.

The distribution patterns observed in the 3D ToF-SIMS images of the 4-mg DEX tablet are further corroborated by the analysis presented in Figure S6, which illustrates the distribution of the components in the 0.5-mg DEX tablet. Similar to the 4-mg tablet, the molecular signal corresponding to DEX is also localized primarily in the upper layers of the 0.5-mg tablet, with decreasing intensity as the sputtering progresses into deeper subsurface

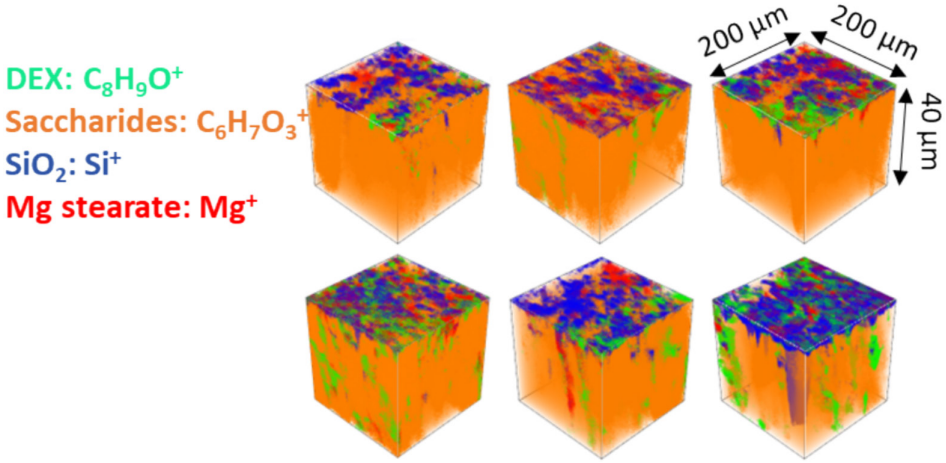

FIGURE 5 | 3D ToF-SIMS images showing the distribution of DEX (green, represented by $C_8H_9O^+$), lactose and starch (orange, represented by $C_6H_7O_3^+$), SiO_2 (blue, represented by Si^+), and Mg stearate (red, represented by Mg^+). 3D ToF-SIMS images were measured for three different 4-mg DEX tablets at two different locations. The depth after 10 800 s of sputtering was determined by using 3D profilometry to be 40 µm.

regions. DEX appears as isolated spots, reflecting the lower active ingredient content compared to that in the 4-mg DEX tablet. A notable distinction between the 4-mg DEX tablet and the 0.5-mg DEX tablet is the different distribution of excipient-related signals.

Compared with the 4-mg DEX tablet, for the 0.5-mg DEX tablet, more SiO_2 is present within the first few micrometer on the surface, which is most likely the reason that a depth of only 15 µm was sputtered off after 10 800 s, compared to a depth of 40 µm that was sputtered off for the DEX tablet containing 4 mg of DEX as GCIB is less effective in sputtering the inorganic material (a lower sputter depth was also noted using XPS, when GCIB sputtering was performed for the 0.5-mg DEX tablet compared to the 4-mg DEX tablet after the same sputtering time periods).

Based on the surface analysis given above, it was shown that although both formulations exhibit heterogeneity in the distribution of the active ingredient, differences in formulation practices and drug concentration may yield variability in the spatial arrangement within the matrix. Comparing these distribution profiles across both tablet formulations provides insights into the effects of drug concentration and excipient composition on tablet heterogeneity, which impacts pharmaceutical performance.

4 | Conclusions

This study provides new insights into the spatial distribution and chemical composition of pharmaceutical tablets by comparing 4-mg and 0.5-mg DEX formulations. The comparison of tablets from different manufacturers highlights the formulation-dependent variability in the distribution of both the active pharmaceutical ingredient and excipients. This study emphasizes the importance of optimizing tablet design to ensure consistent drug release profiles, stability, and performance across different batches and formulations.

The 4-mg and 0.5-mg DEX tablets show heterogeneous surface topographies and morphologies with similar overall roughness values. However, imaging reveals subtle local differences, indicating that the distribution of tablet constituents varies at different places on the tablets and between the two formulations. These differences in surface texture may have implications for tablet uniformity and drug release behavior.

XPS results reveal formulation-dependent differences in surface chemistry. For the 4-mg tablet, the presence of an intense F 1s signal confirms that most of the active ingredient is located in the upper layers, with sputtering removing surface contaminants and exposing underlying excipients. In contrast, the 0.5-mg tablet shows additional Na and Cl signals and a higher proportion of oxidized carbon species at the surface, indicating different excipient compositions compared to the 4-mg DEX tablet. These differences highlight how variations in formulation impact the elemental distribution and chemical states on tablet surfaces. For the 0.5-mg DEX tablet, XPS has a too high a detection limit to be able to detect the F 1s signal due to the low overall F surface atomic concentration, underlining its limiting surface sensitivity for detecting such low surface concentrations. On the other hand, ToF-SIMS provided molecular-specific information that enabled the identification of characteristic ion fragments of DEX, even at low concentrations.

ToF-SIMS identified characteristic DEX ion fragments based on the DEX predicted fragmentation pattern, and MCR confirmed the uniqueness of particular signals. The most intense marker was identified to be the signal for $C_8H_9O^+$ at m/z 121.07, which was used for 3D imaging of the spatial distribution of DEX.

By employing molecular-specific signals for DEX and tablet excipients, it was shown that the 4-mg DEX tablet exhibits a heterogeneous distribution of DEX and tablet excipients, with the active ingredient primarily located at the surface and extending into subsurface regions. In contrast, the 0.5-mg DEX tablet shows DEX confined to isolated spots, reflecting differences in both drug loading and formulation practices from different manufacturers.

These results offer new insights into the spatial distribution of the active ingredients and excipients in DEX tablets and show the importance of surface analytical techniques in pharmaceutical research. The ability to correlate formulation heterogeneity with manufacturing practices and drug release behavior could have significant implications for quality control and the optimization of tablet performance.

Author Contributions

Conceptualization: Matjaž Finšgar. Data curation: Matjaž Finšgar. Formal analysis: Matjaž Finšgar. Funding acquisition: Matjaž Finšgar. investigation: Matjaž Finšgar. Methodology: Matjaž Finšgar. Project administration: Matjaž Finšgar. Resources: Matjaž Finšgar. Software: Matjaž Finšgar. Validation: Matjaž Finšgar. Visualization: Matjaž Finšgar. Roles/writing - original draft: Matjaž Finšgar. Writing - review and editing: Matjaž Finšgar.

Acknowledgments

The Slovenian Research Agency supported the work (Grant Nos. P2-0118 and J1-4416). The project is cofinanced by the Republic of Slovenia, the Ministry of Higher Education, Science and Innovation, and the European Union under the European Regional Development Fund.

Conflicts of Interest

The author declares no conflicts of interest.

Data Availability Statement

The data that support the findings of this study are available on request from the corresponding author. The data are not publicly available due to privacy or ethical restrictions.

References

1. S. Abdoul-Azize, R. Hami, G. Riou, et al., "Glucocorticoids Paradoxically Promote Steroid Resistance in B Cell Acute Lymphoblastic Leukemia Through CXCR4/PLC Signaling," *Nature Communications* 15, no. 1 (2024): 4557.

2. L. P. A. Neyton, R. K. Patel, A. Sarma, et al., "Distinct Pulmonary and Systemic Effects of Dexamethasone in Severe COVID-19," *Nature Communications* 15, no. 1 (2024): 5483.

3. C. S. Jansen, M. S. Pagadala, M. A. Cardenas, et al., "Pre-Operative Stereotactic Radiosurgery and Peri-Operative Dexamethasone for Resectable Brain Metastases: A Two-Arm Pilot Study Evaluating Clinical Outcomes and Immunological Correlates," *Nature Communications* 15, no. 1 (2024): 8854.

4. Q. Hu, Y. Liu, Q. Yue, et al., "Lenalidomide-Induced Pure Red Cell Aplasia Is Associated With Elevated Expression of MHC-I Molecules on Erythrocytes," *Nature Communications* 15, no. 1 (2024): 10131.

5. O. Nadeem, M. P. Aranha, R. Redd, et al., "Deeper Response Predicts Better Outcomes in High-Risk-Smoldering-Myeloma: Results of the I-PRISM Phase II Clinical Trial," *Nature Communications* 16, no. 1 (2025): 358.

6. K. Battiston, I. Parrag, M. Statham, et al., "Polymer-Free Corticosteroid Dimer Implants for Controlled and Sustained Drug Delivery," *Nature Communications* 12, no. 1 (2021): 2875.

7. R. Águas, A. Mahdi, R. Shretta, et al., "Potential Health and Economic Impacts of Dexamethasone Treatment for Patients With COVID-19," *Nature Communications* 12, no. 1 (2021): 915.

8. L. Qu, Q. Zhou, T. Gengenbach, et al., "Investigation of the Potential for Direct Compaction of a Fine Ibuprofen Powder Dry-Coated With Magnesium Stearate," *Drug Development and Industrial Pharmacy* 41, no. 5 (2015): 825–837.

9. J. Pajander, K. B. Haugshøj, K. Bjørneboe, P. Wahlberg, and J. Rantanen, "Foreign Matter Identification From Solid Dosage Forms," *Journal of Pharmaceutical and Biomedical Analysis* 80 (2013): 116–125.

10. J. E. Topolski, H. M. Sheng, C. Moore, et al., "Leveraging ToF-SIMS Imaging to Investigate Tenofovir Disoproxil Fumarate Degradation at Excipient Interfaces in Oral Compressed Tablets," *Journal of Pharmaceutical and Biomedical Analysis* 239 (2024): 115863.

11. M. Finšgar, "Mapping Active Pharmaceutical Ingredients Distributions in Tablets Using Time-of-Flight Secondary Ion Mass Spectrometry With Multivariate Curve Resolution," *Microchemical Journal* 207 (2024): 112156.

12. M. Finšgar, "From Surface to Core: Comprehensive ToF-SIMS Insights Into Pharmaceutical Tablet Analysis," *Microchemical Journal* 202 (2024): 110835.

13. A. M. Belu, M. C. Davies, J. M. Newton, and N. Patel, "TOF-SIMS Characterization and Imaging of Controlled-Release Drug Delivery Systems," *Analytical Chemistry* 72, no. 22 (2000): 5625–5638.

14. J. An, 2013. Time of Flight Mass Spectrometry of Pharmaceutical Systems [PhD Thesis], University of Nottingham.

15. S. Ghazali, A. Baalbaki, W. B. Karroum, A. Bejjani, and A. Ghauch, "Investigating Naproxen Removal From Pharmaceutical Factory Effluents Using UVA/MIL-88-A/PS and Solar/MIL-88-A/PS Systems," *Environmental Science: Advances* 3, no. 1 (2024): 119–131.

16. Q.-B. Liu, J. Liu, J.-G. Lu, et al., "Quantitative 1H NMR With Global Spectral Deconvolution Approach for Quality Assessment of Natural and Cultured Cordyceps Sinensis," *Journal of Pharmaceutical and Biomedical Analysis* 235 (2023): 115603.

17. M. Majrashi, A. Kotowska, D. Scurr, J. M. Hicks, A. Ghaemmaghami, and J. Yang, "Sustained Release of Dexamethasone From 3D-Printed Scaffolds Modulates Macrophage Activation and Enhances Osteogenic Differentiation," *ACS Applied Materials & Interfaces* 15, no. 49 (2023): 56623–56638.

18. J. Mains, C. G. Wilson, and A. Urquhart, "ToF-SIMS Analysis of Dexamethasone Distribution in the Isolated Perfused Eye," *Investigative Ophthalmology & Visual Science* 52, no. 11 (2011): 8413–8419.

19. R. Mitchell, N. L. Marzolini, S. A. Hancock, A. M. Harridance, and D. P. Elder, "The Use of Surface Analysis Techniques to Determine the Route of Manufacture of Tablet Dosage Forms," *Drug Development and Industrial Pharmacy* 32, no. 2 (2006): 253–261.

20. C. Al-Karawi and C. S. Leopold, "A Comparative Study on the Sticking Tendency of Ibuprofen and Ibuprofen Sodium Dihydrate to Differently Coated Tablet Punches," *European Journal of Pharmaceutics and Biopharmaceutics* 128 (2018): 107–118.

21. N. Kaur, G. Haugstad, and R. Suryanarayanan, "Use of Atomic Force Microscopy (AFM) to Monitor Surface Crystallization in Caffeine-Oxalic Acid (CAFOXA) Cocrystal Compacts," *International Journal of Pharmaceutics* 609 (2021): 121196.

22. A. Bártová, R. Gabriel, B. B. Prudilová, E. Otyepková, L. Malina, and M. Otyepka, "Controlled Nucleation of Crystallization Process as an Efficient Tool to Tune the Properties of Corticosteroid API," *Powder Technology* 402 (2022): 117334.

23. S. Duangjit and P. Kraisit, "Optimization of Orodispersible and Conventional Tablets Using Simplex Lattice Design: Relationship Among Excipients and Banana Extract," *Carbohydrate Polymers* 193 (2018): 89–98.

24. T. Gross, M. Ramm, H. Sonntag, W. Unger, H. M. Weijers, and E. H. Adem, "An XPS Analysis of Different SiO2 Modifications Employing a

C 1s as Well as an Au 4f7/2 Static Charge Reference," *Surface and Interface Analysis* 18, no. 1 (1992): 59–64.

25. L. Wang, G. Ren, W. Xie, J. Zhang, D. Pan, and S. Wang, "Simple and Facile Synthesis of Single-Crystal CeO2 Abrasives and Its Highly Efficient Removal Mechanism on SiO2 Film," *Applied Surface Science* 654 (2024): 159510.

26. F. Guan, L. R. Soma, Y. Luo, C. E. Uboh, and S. Peterman, "Collision-Induced Dissociation Pathways of Anabolic Steroids by Electrospray Ionization Tandem Mass Spectrometry," *Journal of the American Society for Mass Spectrometry* 17, no. 4 (2006): 477–489.

27. J.-P. Antignac, B. Le Bizec, F. Monteau, F. Poulain, and F. André, "Collision-Induced Dissociation of Corticosteroids in Electrospray Tandem Mass Spectrometry and Development of a Screening Method by High Performance Liquid Chromatography/Tandem Mass Spectrometry," *Rapid Communications in Mass Spectrometry* 14, no. 1 (2000): 33–39.

28. F. J. Brown and C. Djerassi, "Mass Spectrometry in Structural and Stereochemical Problems. 254. Elucidation of the Course of the Electron Impact Induced Fragmentation of .Alpha.,.Beta.-Unsaturated 3-Keto Steroids," *Journal of the American Chemical Society* 102, no. 2 (1980): 807–817.

29. Y. Y. Lin and L. L. Smith, "Chemical Ionization Mass Spectrometry of Steroids and Other Lipids," *Mass Spectrometry Reviews* 3, no. 3 (1984): 319–355.

30. M. W. F. Nielen, J. J. P. Lasaroms, P. P. J. Mulder, J. Van Hende, J. A. van Rhijn, and M. J. Groot, "Multi Residue Screening of Intact Testosterone Esters and Boldenone Undecylenate in Bovine Hair Using Liquid Chromatography Electrospray Tandem Mass Spectrometry," *Journal of Chromatography. B, Analytical Technologies in the Biomedical and Life Sciences* 830, no. 1 (2006): 126–134.

31. O. J. Pozo, J. Marcos, X. Matabosch, R. Ventura, and J. Segura, "Using Complementary Mass Spectrometric Approaches for the Determination of Methylprednisolone Metabolites in Human Urine," *Rapid Communications in Mass Spectrometry* 26, no. 5 (2012): 541–553.

32. K. E. Arthur, J.-C. Wolff, and D. J. Carrier, "Analysis of Betamethasone, Dexamethasone and Related Compounds by Liquid Chromatography/Electrospray Mass Spectrometry," *Rapid Communications in Mass Spectrometry* 18, no. 6 (2004): 678–684.

33. T. Cairns, E. G. Siegmund, J. J. Stamp, and J. P. Skelly, "Liquid Chromatography Mass Spectrometry of Dexamethasone and Betamethasone," *Biomedical Mass Spectrometry* 10, no. 3 (1983): 203–208.

34. C. J. W. Brooks, A. W. Johnson, and J. H. Beynon, "Some Aspects of Mass Spectrometry in Research on Steroids," *Philosophical Transactions of the Royal Society of London. Series A, Mathematical and Physical Sciences* 293, no. 1400 (1979): 53–67.

35. K. Fluri, L. Rivier, A. Dienes-Nagy, et al., "Method for Confirmation of Synthetic Corticosteroids in Doping Urine Samples by Liquid Chromatography–Electrospray Ionisation Mass Spectrometry," *Journal of Chromatography A* 926, no. 1 (2001): 87–95.

36. J. Haneef, M. Shaharyar, A. Husain, et al., "Application of LC–MS/MS for Quantitative Analysis of Glucocorticoids and Stimulants in Biological Fluids," *Journal of Pharmaceutical Analysis* 3, no. 5 (2013): 341–348.

37. M. Finšgar and K. A. Kravanja, "Forensic Differentiation of Blue Pen Inks Using Time-of-Flight Secondary Ion Mass Spectrometry and Multivariate Statistical Methods," *Microchemical Journal* 205 (2024): 111425.

38. L. Bernard, R. Crockett, and M. Kawecki, "Monosaccharides: A ToF-SIMS Reference Spectra Database. II. Positive Polarity," *Surface Science Spectra* 26, no. 2 (2019): 025002, https://doi.org/10.1116/1.5125103.

Supporting Information

Additional supporting information can be found online in the Supporting Information section.